ELSEVIER

Contents lists available at ScienceDirect

Environmental Research

journal homepage: www.elsevier.com/locate/envres





Excitable systems: A new perspective on the cellular impact of elongate mineral particles

Shuyao Gu ^a, Abby Bull ^{a,b}, Jeneh K. Perry ^c, Amilee Huang ^d, Matt J. Hourwitz ^e, Mona Abostate ^e, John T. Fourkas ^{b,e}, Andrey A. Korchevskiy ^f, Ann G. Wylie ^g, Wolfgang Losert ^{a,b,*}

- ^a Department of Physics, University of Maryland, College Park, MD 20740, United States
- ^b Institute for Physical Science and Technology, University of Maryland, College Park, MD 20740, United States
- c CCDC Army Research Laboratory, Weapons and Material Research Directorate, 6300 Rodman Road, Aberdeen, Proving Ground, MD 21005, United States
- ^d Department of Biology, University of Maryland, College Park, MD 20740, United States
- ^e Department of Chemistry and Biochemistry, University of Maryland, College Park, MD 20740, United States
- f Chemistry & Industrial Hygiene, Inc., 5420 Ward Road, Suite 100, Arvada, CO 80002, United States
- 8 Laboratory for Mineral Deposits Research, Department of Geology, University of Maryland, 8000 Regents Dr., College Park, MD 20742, United States

ARTICLE INFO

Keywords: Elongate mineral particles Esotaxis Immune cells Cytoskeletal activity

ABSTRACT

We investigate how the geometry of elongate mineral particles (EMPs) in contact with cells influences esotaxis, a recently discovered mechanism of texture sensing. Esotaxis is based on cytoskeletal waves and oscillations that are nucleated, shaped, and steered by the texture of the surroundings. We find that all EMPs studied trigger an esotactic response in macrophages, and that this response dominates cytoskeletal activity in these immune cells. In contrast, epithelial cells show little to no esotactic response to the EMPs. These results are consistent with the distinct interactions of both cell types with ridged nanotopographies of dimensions comparable to those of asbestiform EMPs. Our findings raise the question of whether narrow, asbestiform EMPs may also dominate cytoskeletal activity in other types of immune cells that exhibit similar esotactic effects. These findings, together with prior studies of esotaxis, lead us to the hypothesis that asbestiform EMPs suppress the migration of immune cells and activate immune signaling, thereby outcompeting signals that would normally stimulate the immune system in nearby tissue.

1. Introduction

Recent studies on elongate mineral particles (EMPs) strongly suggest that the geometry of amphibole EMPs is more important than the mineral composition in causing adverse health effects, in particular when the fibers have diameters less than 250 nm, lengths greater than 5 μm , and an aspect ratio of at least 3:1 (Wylie et al., 2020). The most carcinogenic category of fibers is crocidolite. Although the diameters of crocidolite fibers are roughly two orders of magnitude smaller than a cell diameter, the fiber width is still more than an order of magnitude larger than the 5 nm diameter of typical proteins in cells. Thus, it is unlikely that the higher potency of 200-nm-diameter fibers compared to 1- μm -diameter fibers could be due to individual receptors or other protein sized cellular sensors.

There has been a significant focus in toxicological studies on

understanding how EMPs are transported through the human respiratory system, in the attempt to explain the carcinogenic potential of thin fibers as being due to the lower probability that such thin fibers can be cleared by the lungs before interacting with sensible tissues, such as the mesothelial layer. Some studies in which asbestiform and nonasbestiform EMPs were implanted directly into animals have shown that thin fibers have a greater adverse impact on health (Stanton, 1981; Pott, 1978; Davis et al., 1991). Similarly, it is well established that both the average width and the potency of amphibole asbestos vary with geological source (Hodgson and Darnton, 2000; Wylie et al., 2020). It is therefore important to understand how cells differentiate the diameters of EMPs.

In this study, we focus on the recently discovered phenomenon of esotaxis, which allows cells to sense the physical properties of their surroundings, including textures on a submicron scale (Sun et al., 2015).

^{*} Corresponding author. Department of Physics, University of Maryland, College Park, MD 20740, United States. E-mail address: wlosert@umd.edu (W. Losert).

Esotaxis is based on the dynamics of polymerization and depolymerization of actin, which create micron-scale, wave-like structures in cells. These dynamic structures are capable of sensing aspects of the microenvironment such as texture (Yang et al., 2022a) and electric fields (Yang et al., 2022b). Actin has long been known to be an essential element in cytoskeletal structure and cellular movement (Horwitz and Webb, 2003). In most previous studies, actin polymerization has been considered to be an output of cellular sensing and decision-making (Pollard and Cooper, 2009; Romero et al., 2020; Svitkina, 2018). Recent work has shown that actin polymerization has intrinsic excitable dynamics, with self-sustaining waves (Yang et al., 2022a) that can be observed in many cell types (Fujiwara et al., 2018; Waizumi et al., 2021). Our prior work showed that in both epithelial cells and neutrophils, actin-polymerization waves can be guided by ridges with submicron widths and micron-scale spacings (Lee et al., 2020). Esotaxis can also affect downstream signaling, for instance by modulating the activation of B cells (Ketchum et al., 2018) and T cells (Wheatley et al., 2022).

In this study, we consider the role of esotaxis in the interaction of cells with rigid amphibole asbestiform EMPs. We introduce a systematic data analysis approach that allows us to compare the esotactic response of cells to asbestiform and nonasbestiform EMPs. We further contrast the behavior of two of the major cell types known to be affected by EMPs, epithelial cells (MCF10A in this work) and macrophages (THP-1 in this work).

2. Materials and methods

2.1. Elongate mineral particles

Multiple asbestiform and non-asbestiform amphibole particle samples were used in this study. Asbestiform minerals naturally crystallize into bundles composed of fibers that are long, thin, flexible, and durable. Non-asbestiform amphiboles produce EMPs upon fragmentation via mechanical forces. Non-asbestiform particles are rigid, and lack the tensile strength of asbestiform varieties (Wylie, 2017). In general, for any given length, asbestiform particles are narrower (i.e., have a higher aspect ratio). No correlation between lung cancer or malignant mesothelioma risk and exposure to non-asbestiform amphiboles has been demonstrated, in contrast to the well-established, high incidence of these diseases upon exposure to amphibole asbestos (Korchevskiy and Wylie, 2021, 2022).

Our experiments used Jamestown, California tremolite, Swansea Lab tremolite, Dornie, Scotland nonasbestiform tremolite, nonasbestiform riebeckite Colorado, and crocidolite asbestos from South Africa. The Jamestown tremolite, Swansea tremolite, and Dornie tremolite samples were those reported by Davis et al. (1991) in a study of peritoneal mesothelioma in rats induced by the implantation of EMPs. Jamestown tremolite, Swansea tremolite, and crocidolite are characterized as asbestiform. The nonasbestiform minerals were ground, and particles were obtained by sieving with dimensions of mostly less than 25 μ m. The asbestiform materials were used as received. The materials were dispersed in distilled water to a concentration of 300 µg/ml. Note that samples with thinner or shorter individual fragments or fibers have a correspondingly higher count of particles/ml than do non-asbestiform particles because non-asbestiform particles have, on average, a larger volume as compared to asbestiform particles. Some of the Dornie tremolite samples and Swansea tremolite suspensions were found to be contaminated with microorganisms, which led to cell death after plating. To sterilize these samples, we autoclaved Dornie tremolite samples and Swansea tremolite suspensions at 121 °C for 25 min (Panasonic MLS-3751 L) under a programmed liquid sterilization procedure. Cell death was not observed after the sterilization.

2.2. Cell lines and cell culture

2.2.1. THP-1

Human THP-1 cells, a leukemia monocytic cell line, were a gift from the laboratory of Iqbal Hamza (University of Maryland, College Park). These cells were maintained at 37 $^{\circ}\text{C}$ in a humid, 95% air/5% CO $_2$ atmosphere in RPMI-1640 medium (ThermoFisher Scientific) containing 10% fetal bovine serum (Gemini Bio-Products) and 55 mM betamercaptoethanol (EMD Millipore). The cells were transfected with the green fluorescent protein LifeAct-GFP, which is a biomarker that selectively binds to F-actin, enabling real-time intercellular observations of actin dynamics.

To observe THP-1 macrophages interacting with EMPs, cells were plated at a 2×10^5 cells/ml density, and phorbol-12-myristate 13-acetate (Sigma-Aldrich) was added to the cell medium, for a final concentration of 100 nM, to trigger differentiation from monocytes to M0 macrophages. After 3 days, the cells became adherent and lost their ability to replicate, displaying the desired macrophage-like morphology. Subsequently, 100 μl of EMP solution was added, and images were obtained 1–2 h after exposure for both EMP-exposed cells and positive controls.

2.2.2. MCF10A

MCF10A LifeAct cells (ATCC), a non-tumorigenic human mammary epithelial cell line, were a gift from the laboratory of Stuart. S. Martin (University of Maryland School of Medicine, Baltimore, MD). These cells were cultured in a medium based on DMEM/F12 with 5% horse serum (both ThermoFisher Scientific), 10 $\mu g/ml$ insulin (ThermoFisher Scientific), 20 ng/ml EGF (Peprotech, Rocky Hill, NJ), 0.5 $\mu g/ml$ hydrocortisone, and 100 ng/ml cholera toxin (both Sigma, St. Louis, MO) as additives. The medium was additionally supplemented with 50 ng/ml puromycin (A.G Scientific, San Diego, CA) for LifeAct GFP selection. The MCF10A LifeAct cell line was incubated at 37 °C in a 95% air/5% CO2 atmosphere and was passaged every 3–4 days (Lee et al., 2020).

Before imaging, a 2 ml solution of MCF10A cells was plated in 35-mm-diameter glass-bottom plates at a density of 10^4 cells/ml. 24 h later, the medium in each well was replaced with fresh, warm medium and 100 μ l of EMP solution. Because epithelial cells did not show a notable response after 1–2 h in preliminary studies, we imaged both EMP-exposed cells and positive controls after 24 h to allow sufficient time for interactions between the minerals and the cells.

2.3. Time-lapse microscopy

Both cell types were imaged by using a PerkinElmer spinning-disk confocal microscope with a $100\times$ objective (0.14 µm/pixel) with 512×512 pixels camera resolution. Time-lapse images of actin dynamics were obtained in confocal fluorescence and bright-field modes. In the fluorescence images, fluorescence intensity directly reflects the actin density. For MCF10A experiments, imaging was performed for 20 m at a frame rate of 3/min. *Z*-stack data with a *z*-step of 0.75 µm were obtained for some MCF10A samples to capture more details regarding how EMPs influence actin dynamics. A *z*-step of 0.75 µm is at the limit of the spinning disk confocal miscroscope used. For THP-1 experiments, fluorescence and bright-field movies were captured at 30 frames/min and 2 frames/min, respectively, for 15 min. Images were captured with a 16-bit Hamamatsu ImagEM X2 EM-CCD camera (C9100–23 B) controlled by Quorum's Volocity software (version 6.4.0).

2.4. Image analysis

The images collected in this paper were all processed and analyzed using ImageJ and/or MATLAB. Feature extraction of EMPs and actin regions was performed in MATLAB by using morphological operations. Asbestiform EMPs usually appear as darker regions in bright-field images, so rescaling and thresholding were used to extract EMP regions.

Note that in some cases, it was necessary to go to a different *z*-plane to improve contrast, as asbestiform EMPs can be difficult to discern when completely in focus. For cases in which *z*-plane images were not available, EMP regions were manually segmented using ImageJ.

3. Results

Immune cells, such as macrophages, neutrophils, and others, act as the body's first line of defense against pathogens, including aberrant cells. As a part of the innate immune system, macrophages are recruited to local tissue sites by chemical, electrical, and physical signaling cues. Actin polymerization waves modulate the mechanical scaffolding of cells and help to direct migration to wound sites (Lee, 2020; Sun, 2015). THP-1 cells exhibit highly active actin dynamics at the cell boundary. These dynamics do not result in protrusions or movement, but rather cause the locations of high actin polymerization activity to vary over time. Additionally, the cells display actin-rich puncta when plated on flat glass substrates, indicating that there is adhesion to such surfaces. When plated on ridged nanotopograppies, the macrophages align with, and extend along, the nanoridges (Fig. 1a). The macrophages do not display actin waves in the valleys of the ridges. Instead, the cells exhibit a heightened level of actin fluorescence at the ridge locations. In contrast, epithelial cells plated on nanoridges exhibit actin signals in the valleys between the ridges, in the form of either straight strips or wiggly lines in the gaps (Lee et al., 2020).

For the qualitative characterization of the different kinds of EMPs used in the experiments, we obtained scanning electron micrographs (SEMs) of each sample (Fig. 2a). Non-asbestiform riebeckite and Dornie tremolite are composed of fragments with small aspect ratios. Crocidolite, Jamestown tremolite, and Swansea Lab tremolite particles, which are all asbestiform, have high aspect ratios. Crocidolite fibers are the thinnest and Swansea Lab tremolite fibers are the thickest among these three.

To study how epithelial cells interact with the EMPs studied here, we obtained bright-field and fluorescence images (Fig. 2a). Fluorescence images of epithelial cells showed little to no actin response to contact with EMPs of any size. The two thinnest asbestiform EMPs, crocidolite and Jamestown tremolite, induced weak actin signals at the fibers. We

did not observe any actin response for cells in contact with the other three EMPs, even upon scanning different *z*-planes of the cells. A representative *z*-stack of images in which Jamestown tremolite fibers are interacting with cells is shown in Fig. 2b. Six *z*-slice images (*z*0 to *z*5) were taken at heights from near the bottom of the cells to near the top, in 0.75-µm increments. Multiple fibers appear in the bright-field image, but the fluorescence image shows actin responding only to a single fiber. Moreover, this actin response occurs at multiple *z*-planes within the cell, and is most prominent in the *z*2 and *z*3 planes. All of the images in Fig. 2 indicate that epithelial cells have weak to no actin response to all EMPs, and only for thinner asbestiform EMPs (crocidolite and Jamestown tremolite) is there some actin activity at the sites of some fibers.

We also obtained bright-field and fluorescence images of macrophages during EMP exposure (Fig. 3). We captured 15-min movies at 2 frames/sec in one single *z*-slice. We analyzed still frames of these movies at 0:00, 5:00, 10:00, and 15:00 min following exposure to visualize how interactions with EMPs influence THP-1 actin dynamics. We observed that macrophages have strong interactions with all of the EMPs, as is indicated by the regions of enhanced actin polymerization located along the EMPs in Fig. 3. In contrast to the epithelial cells, macrophages exhibit a similar response to all five of the EMP samples tested here.

To quantify the actin response of different cells to various EMPs, we created an image-segmentation workflow to identify the EMP regions of interest (ROIs). Using morphological operations, we generate a binary mask of the ROIs with EMPs from the bright-field image (Fig. 4a). The corresponding fluorescence image is used to generate a binary mask of the cell regions. By adding or subtracting these two masks, we create masks for ROIs with and without EMPs. Applying these masks to the fluorescence images, we obtain fluorescence images for ROIs in cells with and without EMPs. The resultant images are used to analyze the difference in the actin activity between the two types of ROI. (Fig. 4b). Note that this segmentation method can be limited by the resolution and magnification of bright-field images. For most EMP samples used here, this method can extract the locations of most mineral fragment samples. However, some fibers from asbestiform crocidolite are too small and too thin to discern in 512×512 pixel images and are difficult to separate from cells in the bright-field images under 100× magnification. The fact that these narrow and light-weight fibers reside at different heights in

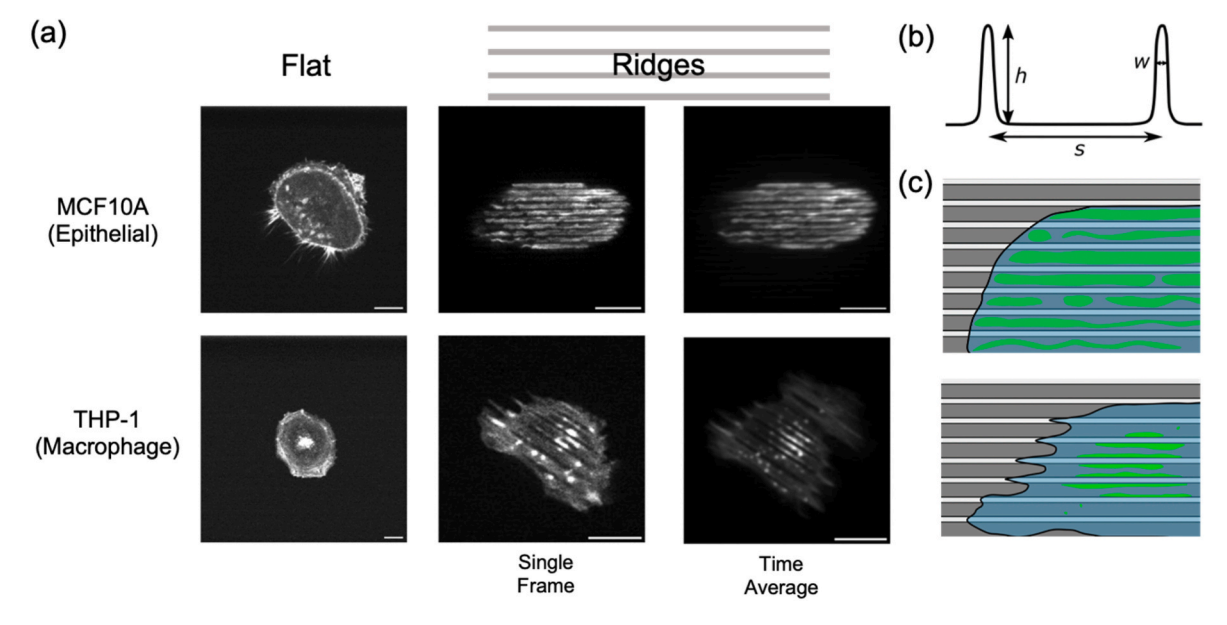


Fig. 1. Macrophages and epithelial cells have different esotactic responses. (a) Fluorescence images of epithelial cells (top) and macrophages (bottom) on different topographies, with the columns displaying images of both cell lines on flat surfaces, on ridged surfaces, and time-averaged images to emphasize the actin dynamics, respectively. The scale bars are 10 μm. (b) A cross-sectional schematic of the ridges. The ridge spacing s is 1.5 μm, the ridge width w is 250 nm, and the ridge height h is 1 μm (Chen, 2019). (c) Cartoons of epithelial cells (top) and macrophages (bottom) on ridges, with blue denoting cell regions and green highlighting the locations of actin activity.

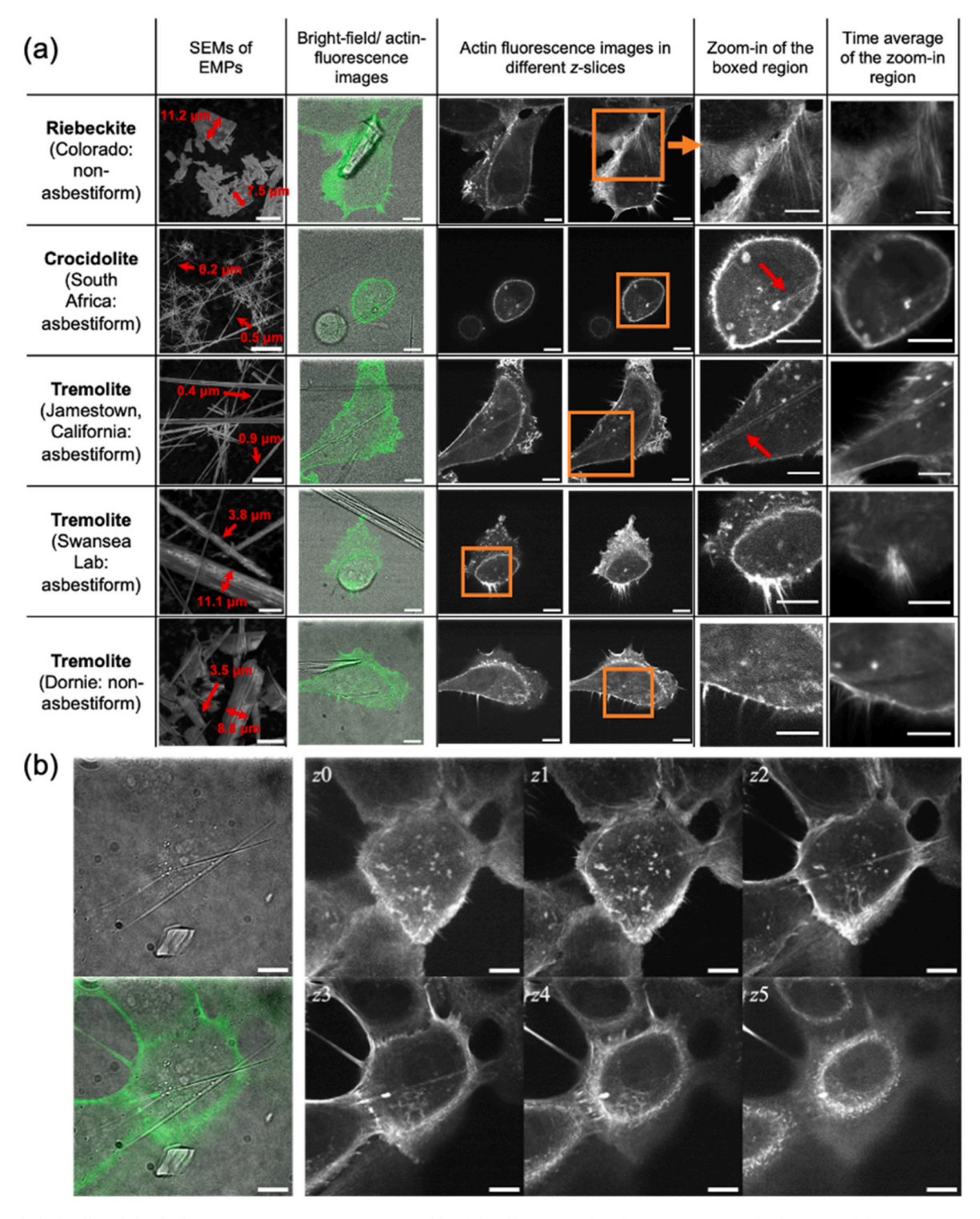


Fig. 2. Epithelial cells exhibit little to no response to EMPs. (a) A table of the all EMPs used in the experiments: Riebeckite, Crocidolite, Jamestown Tremolite, Swansea Lab Tremolite, and Dornie Tremolite. For each type of EMP, a sample SEM is provided, with width measurements of two of the particles labeled in red. Overlays of bright-field (grey) and actin-fluorescence (green) images in the second column show the actin activity relative to the locations of the EMPs. A zoomed-in image of the marked orange box is provided in the next column. Actin-fluorescence images at a single time point are shown for two different heights (0.75 μm apart). The final two columns show single-time-point and time-averaged images of the zoomed-in, orange-boxed region, respectively. (b) Representative bright-field (top left), a bright-field/actin-fluorescence composite images (bottom left), and actin images (z0-z5) at different heights (with a 0.75 μm step) are shown for Jamestown tremolite interacting with epithelial cells. z0 is near the bottom of the cell and subsequent images approach the top. The scale bars are 10 μm.

the cells, combined with the greater number of fibers interacting with individual cells, lead to imprecise masking (Supplementary Fig. 1) and prevent quantification. Therefore, only three kinds of tremolite and one non-asbestiform Riebeckite sample are used for the following

quantification analysis. After generating the segmentation masks, we first compared the time average of the actin fluorescence intensity of ROIs with and without EMPs for four EMP samples used. The excess average actin intensity is the difference in the average actin intensities in

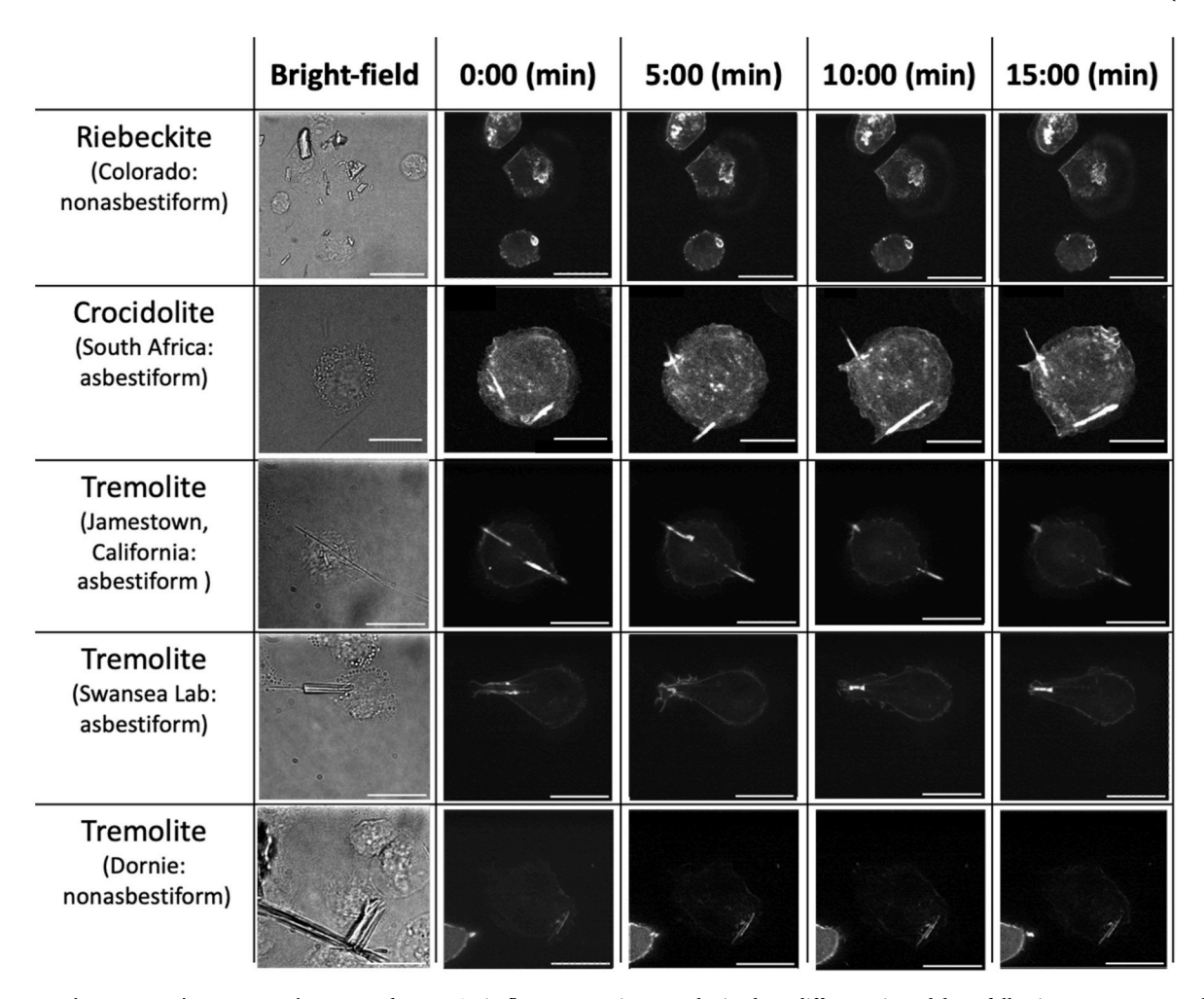


Fig. 3. EMPs trigger esotatic response in macrophages. Actin-fluorescence images obtained at different time delays following exposure to asbestiform (Crocidolite, Tremolite: Jamestown and Swansea Lab) and non-asbestiform (riebeckite and tremolite: Dornie) EMPs. The bright-field images indicate the locations of the particles relative to the macrophages. The scale bars are $30 \mu m$.

ROIs with and without EMPs, divided by the average actin intensity in ROIs without EMPs. Values above zero correspond to cell movies in which the actin fluorescence is brighter than in other areas of the cells. Epithelial cells have excess actin intensity values close to zero, indicating that the actin fluorescence intensity in regions of the cells with EMPs is similar to that in regions without EMPs. In other words, epithelial cells do not have a significant actin response to the EMPs investigated here. In contrast, macrophages exhibit higher excess average actin intensity for EMPs from the asbestiform Jamestown sample. This observation indicates that macrophages have a stronger actin response to some asbestiform EMPs as compared to epithelial cells.

We also investigated the brighter parts of the regions of cells with and without EMPs by finding the highest 5% of actin intensity values (Fig. 4c). We calculated the ratio of the probabilities that the brightest pixels are in ROIs with EMPs compared to elsewhere in the cell. This measure describes how likely it is that the brightest pixels lie near EMPs: A value of 1 means that both are equally likely, and higher values represent a greater likelihood of the brightest actin fluorescence pixels being near EMPs. For both cell lines and all EMP samples, only macrophages interacting with Jamestown tremolite showed a higher percentage of brighter actin signals near EMP as compared to the rest of the cell. Fig. 4b and c indicate that the EMP sample with thinner fibers, Jamestown tremolite, triggers the strongest actin polymerization response by both measures for the EMPs tested.

We also created representative time-evolution images of both cell lines interacting with Jamestown tremolite to visualize the dynamics of actin (Fig. 4d). The image sequence is spectrally time coded; the initial frames are coded in blue, and the final frames are coded in red. The white regions in the composite images indicate regions in which the actin dynamics are stationary, whereas the regions with different colors are locations of transient actin dynamics. Macrophages exhibit a higher degree of actin dynamics at the locations of EMPs, as indicated by the arrows in the figure. The actin dynamics at EMP locations in epithelial cells are subtle, with the majority of actin occurring at the cell boundaries.

4. Discussion

In this study, we showed that EMPs can trigger actin waves in cells (Figs. 2 and 3), indicating a cell's capability of detecting the change in local topography caused by the presence of EMPs. This actin response to EMPs is dependent on both the cell type and the mineral sample. Figs. 2–4 indicate that, in general, epithelial cells have a weaker (or no) response to all types of EMPs than do the macrophages, the latter of which respond strongly to the presence of all of the EMPs tested here.

The different types of EMPs tested here triggered different amounts of actin polymerization. The thinner asbestiform tremolite samples elicited the strongest response. Among the three types of tremolites used in this study, Jamestown tremolite, which has the thinnest fibers, led to the most heightened actin signals. Crocidolite, another EMP with thin fibers, also triggered a stronger actin response in both epithelial cells and macrophages as compared to that triggered by EMPs with broader

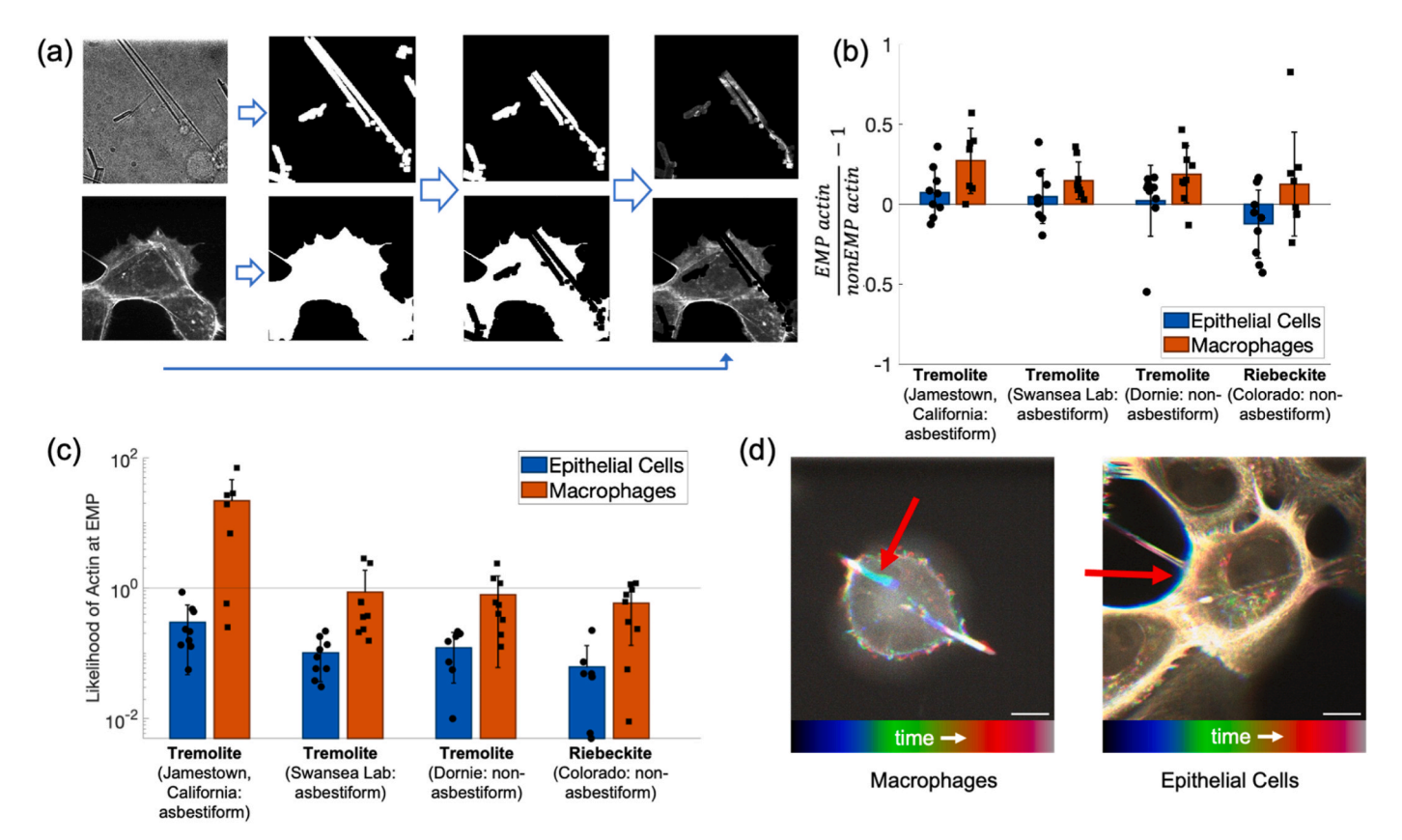


Fig. 4. Narrow asbestiform EMPs dominate cytoskeletal activity in macrophages. (a) Segmentation workflow for image analysis. A bright-field image is used to create a mask for EMP segmentation. The corresponding fluorescence image is used to create a mask to segment cell regions (left half). The EMP-segmentation and cell-segmentation masks are added/subtracted to generate masks for the cell regions with EMPs (top) and without EMPs in cells (bottom). By combining these masks with the original actin images, we can obtain actin images at the sites in cells with EMPs (top) and without EMPs in cells (bottom). Due to the image resolution, this workflow has limitations when applied to asbestiform crocidolite images, so data from this material were excluded in the following quantification analysis. (b) The average actin intensity in regions without EMPs was subtracted from the intensity in regions with EMPs frame-wise over the length of the movies to calculate the excess average actin intensity for epithelial cells (blue) and macrophages (orange). Each marker represents one movie of cells interacting with EMPs. (c) We identified the pixels with the 5% highest fluorescence intensity and calculated what fraction of these pixels is located near EMPs. (d). Time-evolution image of a macrophage (left) and epithelial cells (right) interacting with Jamestown tremolite. Both images were generated from image sequences covering 800 s. The scale bars are 10 μ m. The error bars in (b) and (c) represent plus or minus one standard deviation across independent replicates. In (c), the negative ends of the error bars are not shown in cases in which they are outside of the range of ratios shown.

widths. These observations are consistent with the width of the fibers playing an important role in triggering actin responses in cells.

Interestingly, the macrophages studied here exhibited enhanced actin activity upon interaction with all of the EMPs studied here. The actin fluorescence signals are brighter at the location of EMPs than along the cell boundary. These results are suggestive of substantial cellular interaction with EMPs, which may impact boundary-shape changes and cell migration. As is the case for epithelial cells, macrophages tend to have a stronger response to thinner fibers than to shorter, wider particles. In particular, the highly asbestiform Jamestown tremolite has higher excess average actin fluorescence intensity and higher likelihood of brightest actin fluorescence pixels in regions of EMPs (Fig. 4). These observations indicate that EMPs may ultimately influence the innate overall migration patterns of macrophages in a manner that depends on EMP morphology.

The strong dependence of the actin response on EMP width and cell type is consistent with our prior observation of the responses of both macrophages (unpublished) and epithelial cells (Lee et al., 2020) to surface textures (Fig. 1). Macrophages have actin signals at the location of individual substrate ridges, whereas epithelial cells respond to the valleys formed between adjacent ridges. For cells sensing local topography, asbestiform EMP fibers appear to be analogous to individual ridges. The widths of the ridges that have been studied in this context (Chen, 2019) are similar to the widths of Jamestown tremolite fibers

(Figs. 1 and 2). The heightened actin activity at the locations of EMPs interacting with macrophages is consistent with the actin polymerization phenotype of these cells on nanoridges. Because epithelial cells sense "valleys," such as the concave structure between adjacent ridges, individual EMP fibers triggers little to no actin response. The slight response of the epithelial cells to the Jamestown tremolite and crocidolite samples may arise from the valleys that form between the narrower fibrils that make up the fiber. These findings suggest that esotaxis, the process of sensing the environment through internal waves (Sun et al., 2015), is a means of predicting how strongly different cell types are affected by the presence of EMPs.

This similarity between the responses of actin dynamics to EMPs and nanotextured surfaces suggests that the response of immune cells to textured surfaces is relevant to understanding the effects of EMPs on the immune system. Recent work has demonstrated that textures of size comparable to asbestiform EMPs drive cytoskeletal waves and activates both B cells and T cells, even when molecular immune signals are absent (Ketchum et al., 2018; Wheatley et al., 2022). This mechanism may allow EMPs not only to inhibit the immune-cell migratory machinery, but may also to trigger immune signaling, guiding other immune cells to the same site. Thus, nearby regions in the mesothelium could experience a weakened immune response, depriving the tissue of the healing power of the immune system. Indeed, severe immunodeficiency was implicated as one of the factors associated with an increased risk of malignant

mesothelioma, even in the absence of known exposure to asbestos (Bianchi and Bianchi, 2008). Thus, we propose that the esotactic response of immune cells to EMPs, which results in suppression of cell migration and immune-cell activation, may divert the body's own defenses against malignancies. This mechanism of indirect carcinogenic action is not predicated on the mineral nature of EMPs, and thus potentially also applies to other elongate particles of comparable geometry. It will therefore be important to characterize the esotactic immune response further and to identify novel approaches that may suppress this immune activation pathway.

Author contribution statement

Shuyao Gu: Data curation, Formal analysis, Software, Investigation, Methodology, Visualization, Writing – original draft, Writing – review & editing. Abby Bull: Investigation, Writing – original draft. Jeneh K. Perry: Investigation, Writing – original draft, Visualization. Amilee Huang: Investigation, Writing – original draft, Matt Hourwitz: Investigation, Mona Abostate: Investigation, John T. Fourkas: Conceptualization, Funding acquisition, Writing – review & editing. Andrey A. Korchevskiy: Validation, Writing – review & editing. Ann G. Wylie: Conceptualization, Resources, Writing – review & editing. Wolfgang Losert: Conceptualization, Funding acquisition, Methodology, Project administration, Writing – original draft, Writing – review & editing

Funding

This work was supported by NSF grant PHY2014151.

Declaration of competing interest

The authors declare that they have no known competing financial interests or personal relationships that could have appeared to influence the work reported in this paper.

Data availability

The data generated in this paper are available from https://doi.org/10.5281/zenodo.7212216

Acknowledgment:

We thank Iqbal Hamza (University of Maryland College Park) for the gift of THP-1 macrophages and Stuart S. Martin (University of Maryland School of Medicine) for the gift of epithelial MCF10A cells.

Appendix A. Supplementary data

Supplementary data to this article can be found online at https://doi.org/10.1016/j.envres.2023.115353.

References

- Bianchi, C., Bianchi, T., 2008. Susceptibility and resistance in the genesis of asbestosrelated mesothelioma. Indian J. Occup. Environ. Med. 12, 57–60.
- Chen, S., et al., 2019. Actin cytoskeleton and focal adhesions regulate the biased migration of breast cancer cells on nanoscale asymmetric sawteeth. ACS Nano 13 (2), 1454–1468.
- Davis, J.M., et al., 1991. Variations in the carcinogenicity of tremolite dust samples of differing morphology. Ann. N. Y. Acad. Sci. 643, 473–490.
- Fujiwara, I., et al., 2018. Polymerization and depolymerization of actin with nucleotide states at filament ends. Biophysical Reviews 10, 1513–1519.
- Horwitz, R., Webb, D., 2003. Cell migration. Curr. Biol. 13, R756-R759.
- Ketchum, C.M., et al., 2018. Subcellular topography modulates actin dynamics and signaling in B-cells. Mol. Biol. Cell 29, 1732–1742.
- Korchevskiy, A.A., Wylie, A.G., 2021. Dimensional determinants for the carcinogenic potency of elongate amphibole particles. Inhal. Toxicol. 33, 244–259.
- Korchevskiy, A.A., Wylie, A.G., 2022. Dimensional characteristics of the major types of amphibole mineral particles and the implications for carcinogenic risk assessment. Inhal. Toxicol. 34, 24–38.
- Lee, R.M., et al., 2020. Quantifying topography-guided actin dynamics across scales using optical flow. Mol. Biol. Cell 31, 1753–1764.
- Pollard, T.D., Cooper, J.A., 2009. Actin, a central player in cell shape and movement. Science 326, 1208–1212.
- Pott, F., 1978. Some aspects on the dosimetry of the carcinogenic potency of asbestos and other fibrous dusts. Staub Reinhalt. Luft 38, 486–490.
- Romero, S., et al., 2020. Actin polymerization downstream of integrins: signaling pathways and mechanotransduction. Biochem. J. 477, 1–21.
- Stanton, 1981. Relation of particle dimension to carcinogenicity in amphibole asbestos and other fibrous minerals. J. Natl. Cancer Inst. 67 (5), 965–975. PMID 6946253.
- Sun, X., et al., 2015. Asymmetric nanotopography biases cytoskeletal dynamics and promotes unidirectional cell guidance. Proc. Natl. Acad. Sci. USA 112, 12557–12562.
- Svitkina, T., 2018. The actin cytoskeleton and actin-based motility. Cold Spring Harbor Perspect. Biol. 10, a018267.
- Waizumi, T., et al., 2021. Polymerization/depolymerization of actin cooperates with the morphology and stability of cell-sized droplets generated in a polymer solution under a depletion effect. J. Chem. Phys. 155, 75–101.
- Wheatley, B.A., et al., 2022. Nanotopography modulates cytoskeletal organization and dynamics during T cell activation. Mol. Biol. Cell 33.
- Wylie, A., 2017. Mineralogy of Asbestos and fibrous erionite. In Current Cancer Research: Asbestos and Mesothelioma, Joseph Testa Ed. Springer, Heidelberg, pp. 11–41.
- Wylie, A.G., et al., 2020. Modeling mesothelioma risk factors from amphibole fiber dimensionality: mineralogical and epidemiological perspective. J. Appl. Toxicol. 40, 515–524.
- Yang, Q., et al., 2022a. Nanotopography Modulates Intracellular Excitable Systems through Cytoskeleton Actuation. Cold Spring Harbor Laboratory.
- Yang, Q., et al., 2022b. Cortical waves mediate the cellular response to electric fields. Elife 11.
- Hodgson, J.T., Darnton, A., 2000. The quantitative risks of mesothelioma and lung cancer in relation to asbestos exposure. Ann Occup Hyg. 44 (8), 565–601. PMID: 11108782